SUPPORTING MATERIAL

Transport by populations of fast and slow kinesins uncovers novel family-dependent motor characteristics important for *in vivo* function

Göker Arpağ,[†] Shankar Shastry,[‡] William O. Hancock,[‡] Erkan Tüzel,[†]

[†]*Department of Physics, Worcester Polytechnic Institute, Worcester, MA, 01609, USA*
[‡]*Department of Biomedical Engineering, The Pennsylvania State University, University Park, PA, 16802, USA*

I Estimation of unloaded velocities from gliding assays

The unloaded motor velocity, v_u, is typically measured by observing the motion of a single kinesin motor labeled with a fluorescent tag or bead as it walks along an immobilized microtubule under zero external load. Alternatively, motor velocity can be measured in a gliding assay by constructing kymographs and measuring the slope as illustrated in Fig. S1. In contrast to the single-motor assay, a kinesin in a gliding assay is always under some load due to the presence of the other motors pulling in either assisting or hindering directions, in addition to the viscous drag due to the microtubule. The gliding velocities observed are therefore expected to underestimate the actual unloaded motor velocity.

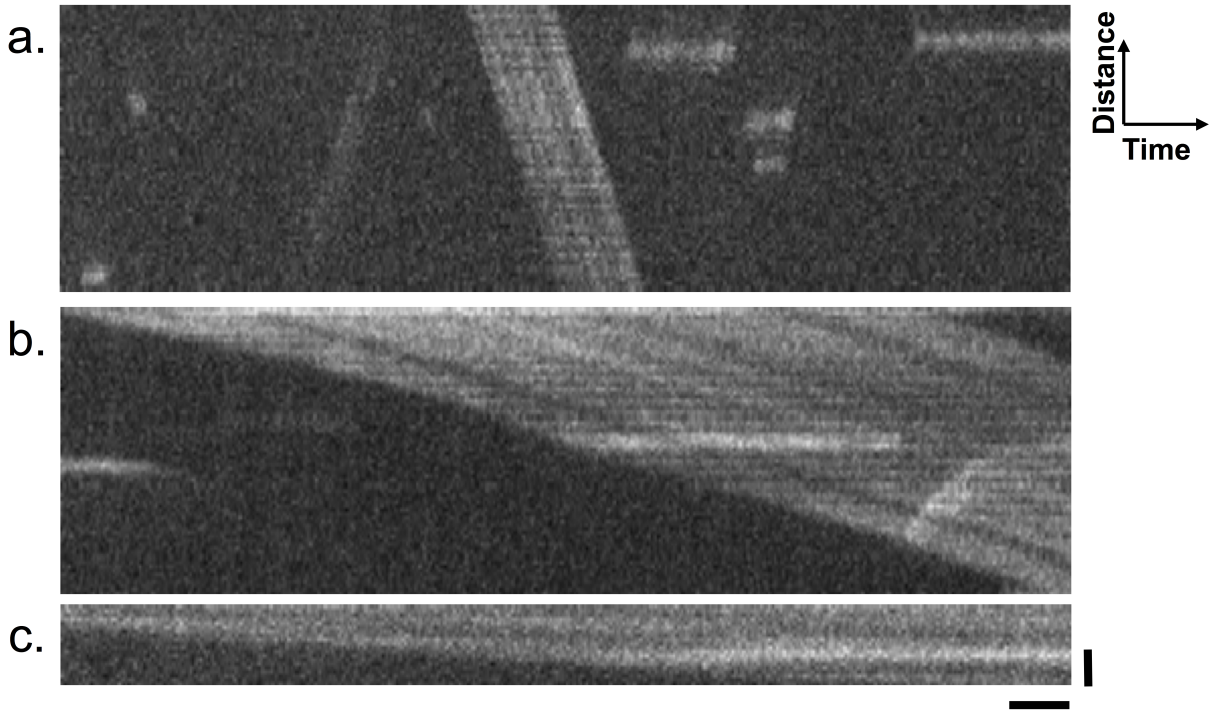

Figure S1: Representative kymographs for kinesin-1/kinesin-5 motor mixing experiments. Kymographs were generated using ImageJ software. Time is represented on the x-axis and distance on the y-axis. Scales shown are 1 s and 1 μm, respectively, on the time and distance axis. (a) Kymograph of 100% kinesin-1. (b) Kymograph of 20% kinesin-1, 80% kinesin-5 mixture. (c) Kymograph of 100% kinesin-5.

In order to estimate the unloaded single-motor velocity of a given motor, we used the simulations to match the experimentally observed gliding velocities for uniform motor populations. Starting with the microtubule velocity

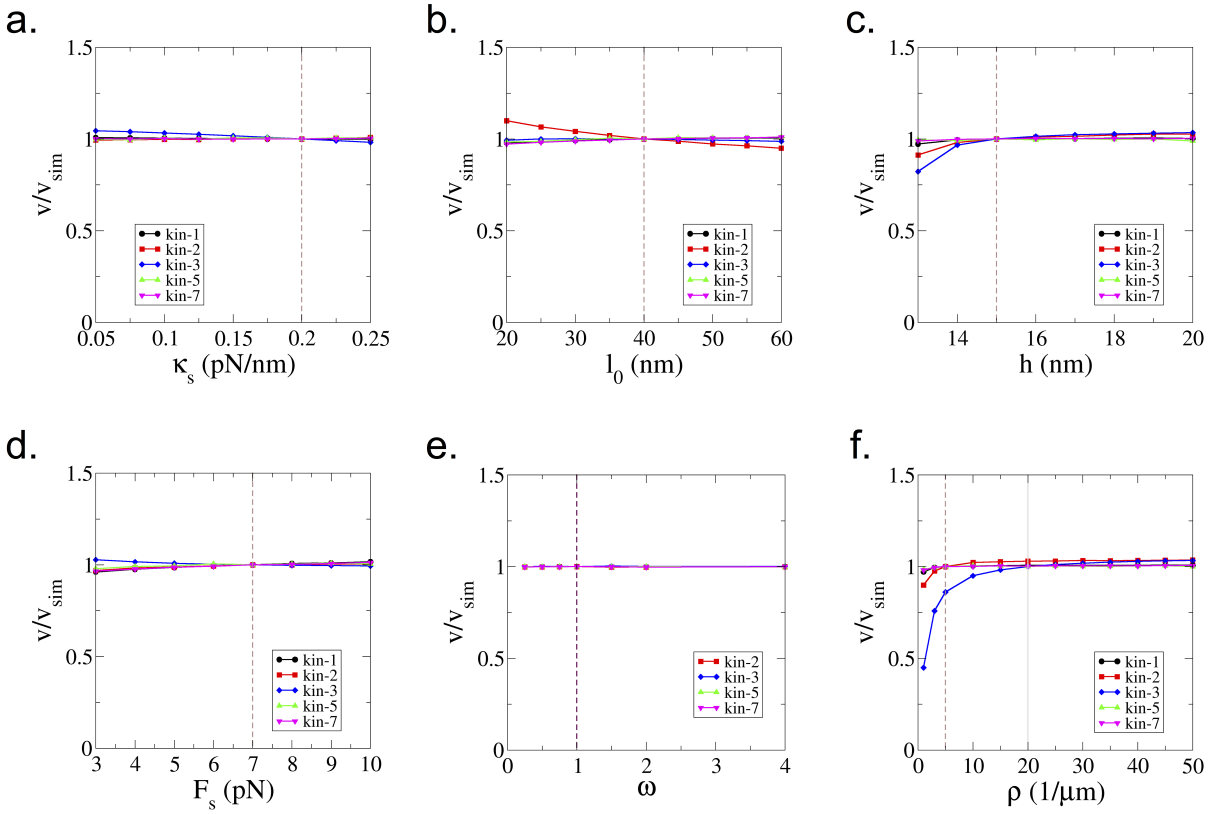

Figure S2: Sensitivity analysis for uniform motor simulations. Dependence of microtubule velocity on the (a) motor compliance κ_s; (b) motor rest length, ℓ_0; (c) height of the microtubule above the surface, h; (d) motor stall force, F_s; (e) form of the motor force-velocity curve (Eq. (8)); and (f) motor density, ρ. In each panel, the vertical dashed line corresponds to the parameter value used in the final simulations, and the resulting simulated gliding velocity is denoted by v_{sim}. In f) all simulations used $\rho = 5\ \mu m^{-1}$, except kinesin-3 simulations, which used $\rho = 20\ \mu m^{-1}$.

from uniform motor population assays (i.e. motor fraction 0 or 1 in Fig. 3), the single-motor velocity, v, was varied incrementally, until the resulting microtubule velocity obtained from the simulations matched the experimental value. The differences between the experimental microtubule gliding velocities and the unloaded single-motor velocities input into the simulations are shown in Table S1. The results show that single-motor velocities were about $1-10\%$ higher than the observed gliding velocity for all motors except kinesin-2, which was lower. Kinesin-2 detaches readily under assisting loads ($k_{\text{off}}(F) = 15\ s^{-1}e^{F/2.0\ pN}$ (Table 1)) and this is the primary mode of detachment even in uniform kinesin-2 assays (Fig. S7b and Movie S2). This effect results in selective detachment of any motors moving slower than the mean, and an overall microtubule gliding velocity that exceeds the single-motor velocity. It is important to note that these results are not sensitive to the choice of parameters such as motor compliance, rest length of the motor tether, distance from the glass, stall force, shape of the force-velocity curve, or motor density (see Fig. S2, and Section II).

II Parameter sensitivity for uniform and mixed-motor assays

In order to investigate the sensitivity of our simulations to the specific choice of parameters, we performed an extensive sensitivity analysis. Parameters include motor compliance κ_s, motor rest length ℓ_0, the height of the microtubule from the surface h, stall force F_s, shape of the force-velocity curve, and motor density ρ. Potential dependencies of the microtubule velocity on these parameters were tested for both uniform and mixed-motor (50/50) assays.

Table S1: The percentage difference between experimentally observed gliding velocities for uniform motor populations and the unloaded single-motor velocities used in the simulations to reproduce these values. Note that experiments for given pairs of motors (i.e. kinesin-1 and kinesin-2) were carried out as a set on a given day so as to minimize experimental variability. Hence, the microtubule velocity for uniform populations (shown in Fig. 3) varies slightly depending on the motor pair.

Motor A	**Motor B**	$v_u^{\mathbf{A}}$ / $v_{\mathbf{exp}}^{\mathbf{A}}$	$v_{\mathbf{u}}^{\mathbf{B}}$ / $v_{\mathbf{exp}}^{\mathbf{B}}$
kinesin-1	kinesin-2	1%	-10%
kinesin-1	kinesin-3	2%	7%
kinesin-1	kinesin-5	2%	3%
kinesin-1	kinesin-7	2%	4%
kinesin-2	kinesin-3	-9%	8%
kinesin-2	kinesin-5	-8%	3%
kinesin-3	kinesin-5	8%	3%
kinesin-3	kinesin-7	8%	4%
kinesin-5	kinesin-7	3%	4%

It has been observed that kinesin-1 motors display non-linear elastic behavior in response to a force, resulting in strain-induced stiffening (1, 2). In order to investigate the role of compliance on the observed gliding velocities, we performed simulations with compliance values ranging from 0.05 pN/nm to 0.25 pN/nm. No dependence on compliance was observed for uniform assays (Fig. S2a), and for most of the mixtures, only a weak dependence was observed (Fig. S3a). One exception was for the kinesin 2-3 mixtures, where the detachment of both motors is very sensitive to load, and so changes in compliance strongly impacted detachment rates. The second exception was motor mixtures that included kinesin-5, where smaller compliances led to slower velocities due to a combination of the faster motor (kinesin-1, kinesin-2 or kinesin-7) taking longer to build up force against the slower kinesin-5, and kinesin-5 remaining attached longer due to its ability to stretch more. This behavior reinforces the idea that kinesin-5 acts like a brake in stabilizing the mitotic spindle from collapse and resisting dynein-mediated microtubule transport in axons (3, 4). Based on these observations, we chose a compliance value of $\kappa_s = 0.2\ pN/nm$.

In the gliding assays being modeled, $\sim$340 amino acid motor domains were followed by 214 amino acids consisting of the dimerization coiled-coil and coil-1 separated by a $\sim$50 residue flexible "swivel" domain (5), and an anti-His antibody adsorbed to the glass surface (Fig. 1a), resulting in an estimated rest length of $\ell_0 \simeq 40\ nm$. The dependence of the observed gliding velocity on the rest length for uniform motors and 50/50 mixtures is shown in Figs. S2b and S3b, respectively. The results show no sensitivity for uniform motor assays, and relatively little sensitivity for mixed motor assays.

The distance that kinesin-1 holds its cargo from the microtubule surface was measured by Kerssemachers et. al., using fluorescence interference contrast microscopy (6). Because all of our motors were fused to the dimerization domain and coil-1 of Drosophila kinesin-1 (residues 346 to 559) (7), we assume that the distance between the microtubule and the glass surface in our gliding assays is the same for every motor, and estimate it to be $h = 15\ nm$. Fig. S2c shows that gliding velocities from simulations using uniform motor populations are insensitive to h, and similar insensitivity was observed for the 50/50 mixtures, as shown in Fig. S3c.

A fit to the experimentally determined kinesin-1 force-velocity curve shown in Fig. 1b yields a stall force of $F_s = 7\ pN$, and we used this value for all the motors in the simulations. We tested the dependence of gliding

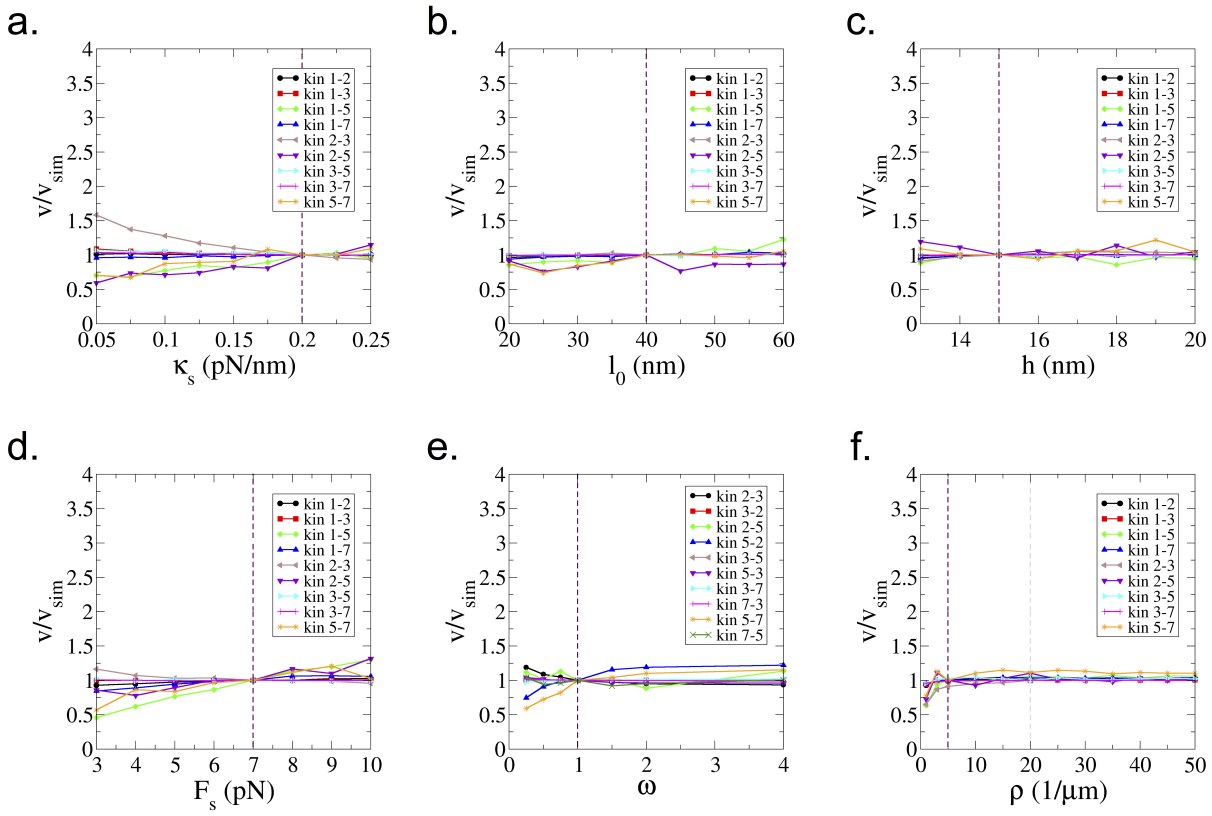

Figure S3: Sensitivity analysis for mixed motor simulations. Dependence of microtubule velocity for 50/50 mixtures on the (a) motor compliance κ_s; (b) motor rest length, ℓ_0; (c) height of the microtubule above the surface, h; (d) motor stall force, F_s; (e) form of the motor force-velocity curve (Eq. (8)); and (f) motor density, ρ. In each panel, the vertical dashed line corresponds to the parameter value used in the final simulations, and the resulting simulated gliding velocity is denoted by v_{sim}. For force-velocity profiles in (e), ω was set to 1 for the first motor in the pair and was varied for the second motor. Because the kinesin-1 profile was taken from experimental data (Fig. 1b), it was excluded from the ω sensitivity analysis. In (f) all simulations used $\rho = 5\ \mu m^{-1}$, except kinesin-3 simulations, which used $\rho = 20\ \mu m^{-1}$.

velocity on stall force for uniform and 50/50 motor mixtures (Figs. S2d and S3d, respectively). For uniform motor populations, velocities were insensitive to F_s (Fig. S2d). For motor mixtures (Fig. S3d), there was generally a similarly flat dependence of velocity on F_s. Two exceptions were combinations of kinesin-5 with kinesin-1 or kinesin-7. Because kinesin-5 is very slow and both kinesin-1 and 7 continue to walk against significant loads, many of these faster motors are operating near stall when pulling on kinesin-5 (see Movies S8 and S14). Hence, this dependence is not surprising. Yardimci *et al.* found nearly identical stall forces between kinesin-7 and kinesin-1 (8), and 7 pN is the best estimate for the kinesin-5 stall forces based on optical trapping studies (9), providing support for our choice of a uniform 7 pN stall force for all motors used in this study. The dependency of the gliding velocity on the shape of the force-velocity relationship was also tested as shown in Figs. S2e and S3e. For uniform populations, velocities were insensitive to the parameter ω, spanning the range from sub-linear to super-linear motors. For motor mixtures, there was generally a flat dependence of velocity on ω, with the exception of the combinations of kinesin-5 with kinesin-2 or kinesin-7 for very small ω values. Once again this dependence is not surprising, given our observations of the weak stall force dependence for these combinations.

Finally, we investigated the dependence of our simulation results on motor density (Fig. S2f and S3f). For both uniform and mixed motor assays, motor density had little effect on the results, with the exception of kinesin-3, the fastest and weakest motor where frequent detachment reduced its effective density. In both the gliding assay

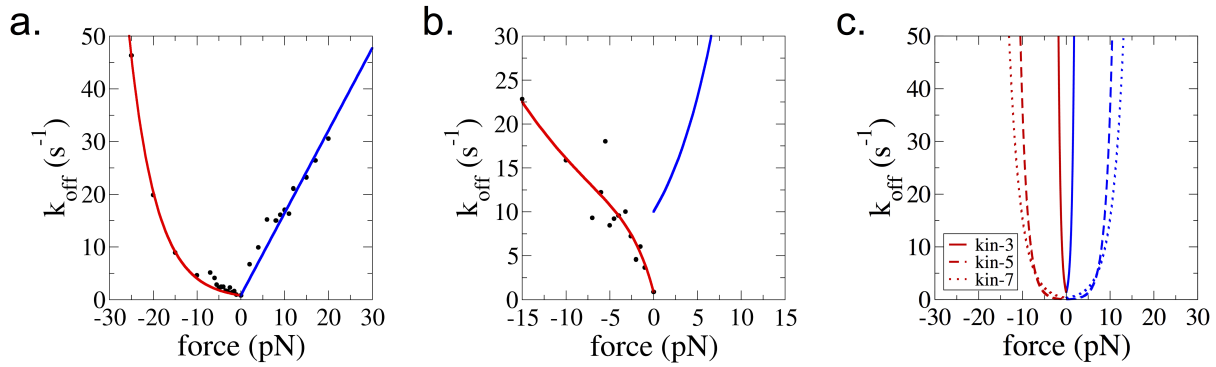

Figure S4: Force dependent off-rates for (a) kinesin-1, (b) kinesin-2, (c) kinesin-3, 5 and 7. Data shown in (a) and (b) are taken from Andreasson (10). Kinesin-1 off-rate is exponential under hindering load, and linear under assisting load. Kinesin-2 off-rate data can be explained by a double exponential under hindering load. Kinesin-2 off-rate under assisting load, and kinesin-3, 5 and 7 off-rates for both cases were determined using simulations. Table 1 shows the explicit forms of the functions used. Red and blue lines denote hindering and assisting loads, respectively.

experiments and the simulations, a sufficiently high motor density was used to ensure that the results do not depend on motor density. Therefore, in the simulations involving kinesin-3 motors we used a motor density of $\rho = 20\ \mu m^{-1}$, and for all other motors the density was chosen to be $\rho = 5\ \mu m^{-1}$ to reduce the computational cost.

III Parameter optimization and estimation of critical detachment force, F_c

Force-dependent off-rates ($k_{\text{off}}(F)$) for kinesin-1 in both hindering and assisting directions (Fig. S4a) were taken directly from single-molecule velocity and run length data (10). $k_{\text{off}}(F)$ for kinesin-2 under hindering loads was taken from the same study (Fig. S4b), but no equivalent experimental data are available for kinesin-2 under assisting loads, because the motor detaches rapidly in this regime. Thus, $k_{\text{off}}(F)$ for kinesin-2 under assisting loads and for kinesin-3, kinesin-5 and kinesin-7 under both hindering and assisting loads were iteratively determined by matching mixed-motor simulation results to experimental data (Figs. S4b and c, and Fig. 3).

The approach to determining unknown F_c values was as follows. For every motor, mixed-motor simulations with every other motor were carried out across a range of F_c values, with each data point being an average of 10 independent realizations. The percent error at each motor fraction (relative to experimental velocities) was calculated and averaged to get the mean percent error for a given motor mixture at a given F_c. This process was repeated until converging on optimum F_c values that gave the lowest error for kinesin-2 in the assisting direction, and kinesin-3, kinesin-5 and kinesin-7 in both directions (Fig. S5).

IV Distribution of instantaneous forces and forces at detachment

In order to develop better mechanistic insight into the underlying motor behavior, we measured the distribution of both instantaneous forces and forces at detachment for all of the uniform and mixed-motor simulations. Shown in Fig. S7 is the fraction of motors that detach under hindering or assisting loads, which is qualitatively similar to the fraction of motors experiencing a hindering or an assisting load at any instantaneous time point in the simulation (Fig. 5). The mean forces, both instantaneous and at the point of detachment, are shown in Fig. S8. The measured detachment forces are almost always larger than the instantaneous forces, reaching values as high as 10 pN. One feature of the data is that kinesin-3 motors, the fastest of the five, almost all detach under hindering loads, while kinesin-5 motors, the slowest of the five, almost always detach under assisting loads. However, due to the propensity of kinesin-3 to detach under load, the mean forces at detachment are lower than for kinesin-5. In general, the magnitudes of the forces scale with F_c, meaning that motors least susceptible to detachment by load stay on to generate the largest loads.

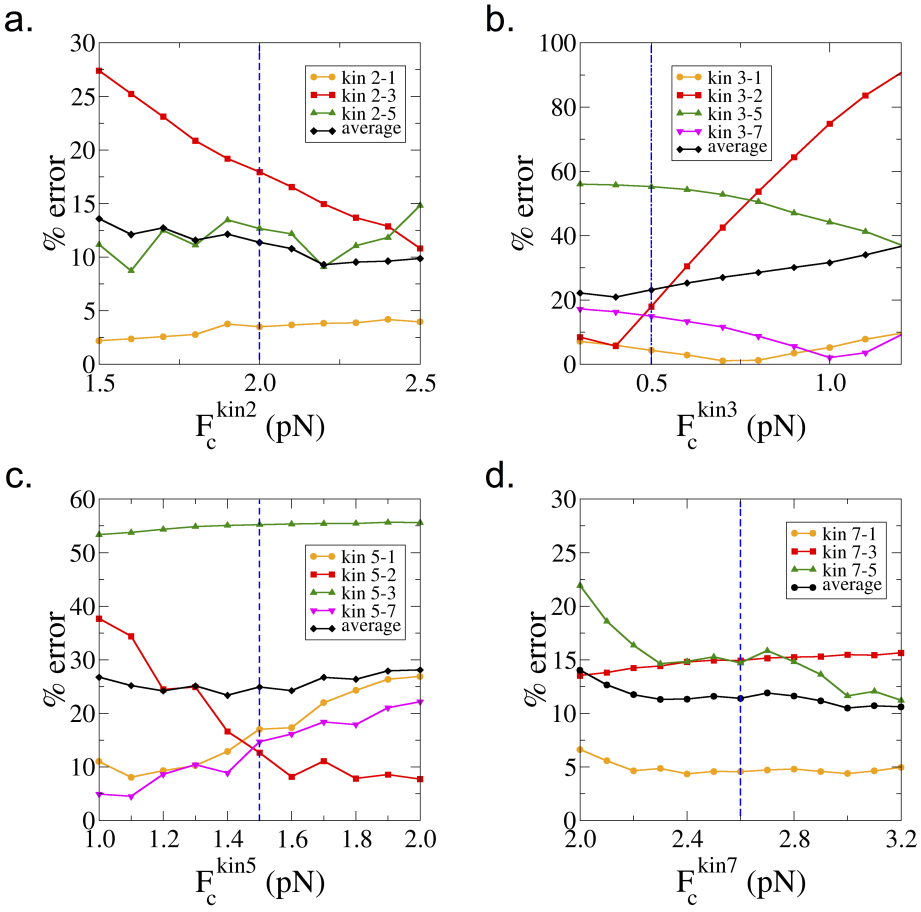

Figure S5: Percent error as a function of the critical force, F_c, for different multi-motor mixtures (a-d). The average error for all motor mixtures for a given motor is shown in black, and vertical dashed lines correspond to the optimum F_c values used in the simulations.

Some insight into the surprisingly broad force distributions in the gliding assay can be achieved by using a simple statistical model to calculate the distribution in velocities of different motors when averaged over their entire run. Neglecting the force dependence of the dissociation rate, the amount of stretch on a given motors tether, d_i, can be written as

$$d_i = v_{MT} \sum_{j=1}^{N_s} T_j - L_i \quad , \tag{S1}$$

where v_{MT} is the speed of the microtubule, T_j is the duration of the jth step of a total of N_s steps, and L_i is the run length of the ith motor. Here $N_s = L_i/\delta$ is the total number of steps the ith motor takes. If the motors are modeled as stochastic steppers, the duration of a given time step and the run lengths will be exponentially distributed, i.e.,

$$P(T_i) = \frac{1}{\tau} e^{-T_i/\tau} \quad , \tag{S2}$$

$$P(L_i) = \frac{1}{\mu} e^{-L_i/\mu} \quad . \tag{S3}$$

Here τ and μ are the mean step times and run lengths, respectively. Assuming a step size of 8 nm, taking the mean association time and run length of a kinesin-1 motor to be 1.27 s and 1 μm, and using an average gliding velocity of 816 nm/s, one can calculate the distribution of distances each motor tether will stretch at the point of detachment

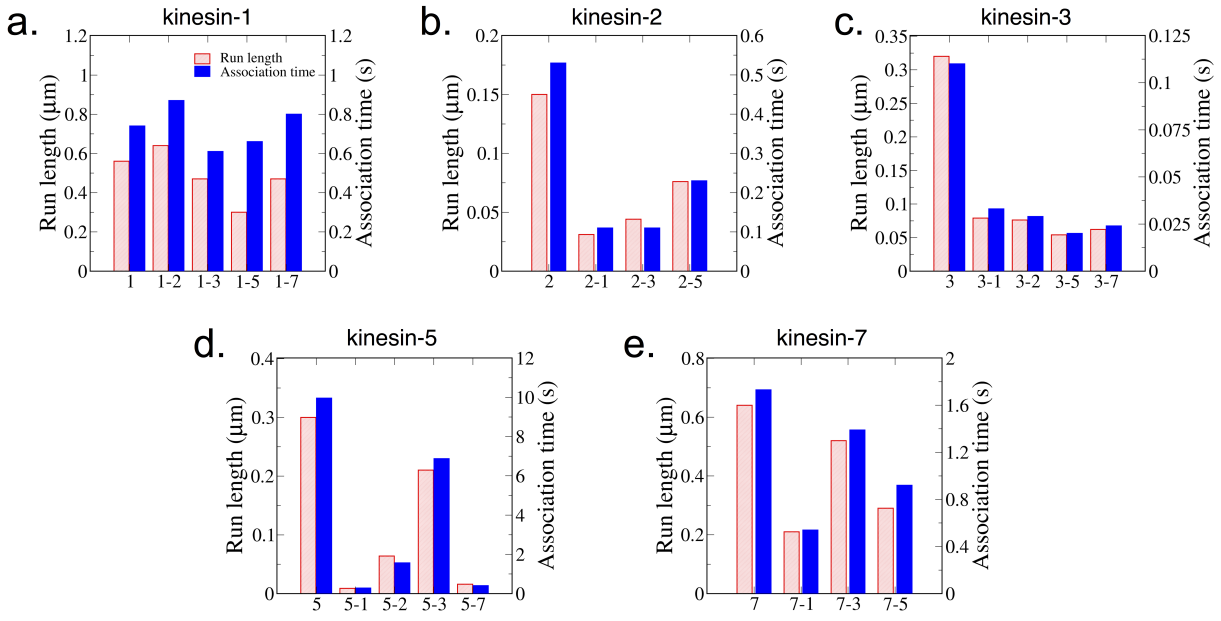

Figure S6: Mean run length and association times for uniform and multi-motor simulations (a-e). Data are used to calculate motor velocities in Fig. 4. Motor mixtures were all 50/50 ratios.

(see Fig. S9a). As shown in Fig. S9b, due to the stochastic nature of stepping, 55% of the motors stretch greater than 40 nm, the resting length of the tether used in our simulations. Furthermore, over a quarter of the motors (27%) are expected to stretch more than 90 nm, the approximate maximum contour length for full-length kinesin-1. Measurements of the randomness parameter for kinesin-1 have suggested that instead of a simple Poisson stepper (giving an exponential distribution of step durations), kinesin-1 is better described by a mechanism involving two sequential rate limiting processes, giving a randomness factor of 0.5 (11). Thus, this simulation was repeated using a randomness of 0.5 by defining the step duration distribution as the sum of two independent exponential distributions with identical mean durations. Using this 0.5 randomness, at the point of detachment 35% of the motors stretched beyond their slack length of 40 nm and 17% of the motors stretch beyond their maximum contour length of 90nm. Hence, even in multi-motor assays using uniform kinesin populations, due to the inherent variability in stepping rate and the relatively long run lengths, motors are expected to stretch and build up large forces. This simple statistical model contrasts with the common assumption that uniform motor populations all walk with similar speeds and thus do not generate considerable motor-motor forces in gliding assays.

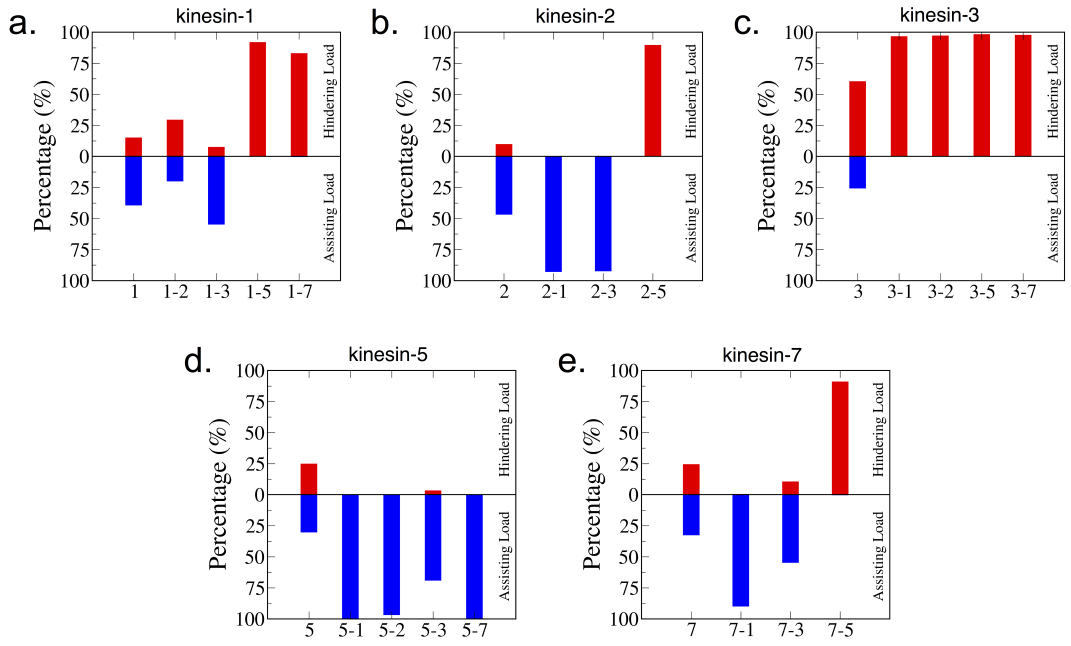

Figure S7: Percentage of motors that detach under non-zero assisting (blue) or hindering (red) loads (a-e). Results for the different motor mixtures are for 50/50 ratios.

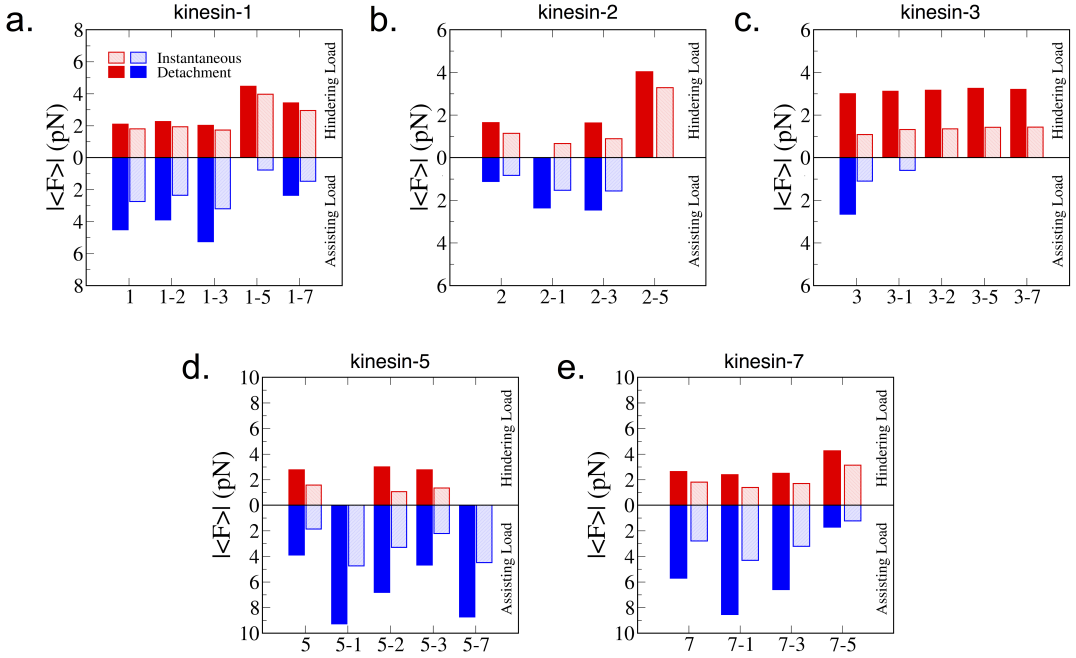

Figure S8: Mean values of instantaneous force and force at detachment for uniform and mixed-motor simulations (a-e). Hindering and assisting loads are grouped separately and average values are shown for both. Motors under zero load, corresponding to motors with tethers less than the rest length of 40 nm are excluded from the calculations. Mixed motor force data corresponds to 50/50 mixtures.

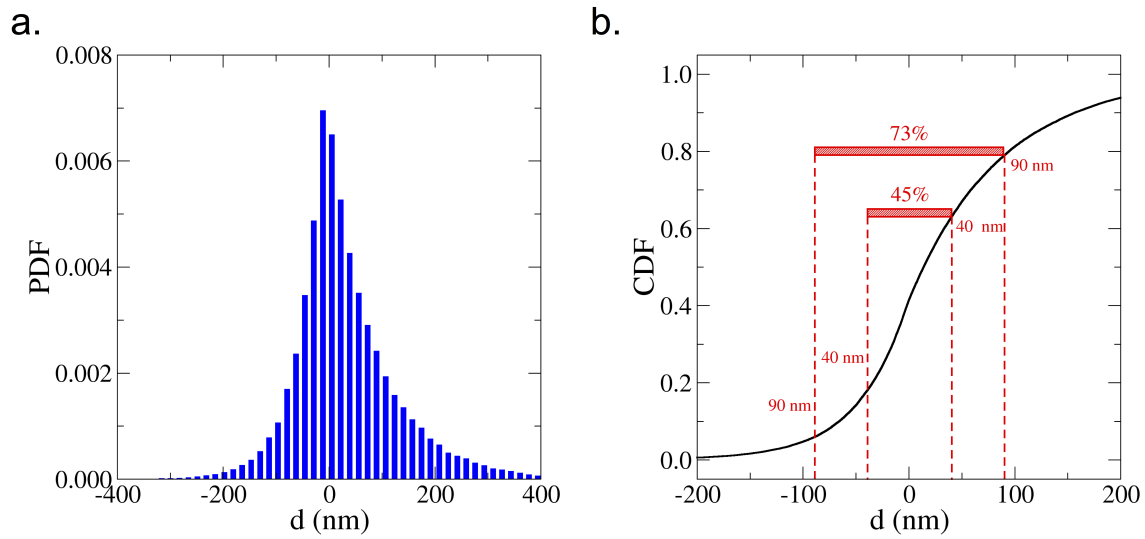

Figure S9: Probability distribution (PDF) and cumulative distribution functions (CDF) for the stretch of a motor tether. Data are from a simulation of a simple Poisson stepper showing the predicted stretch of the tether at the point of detachment.

V Additional supplementary figures

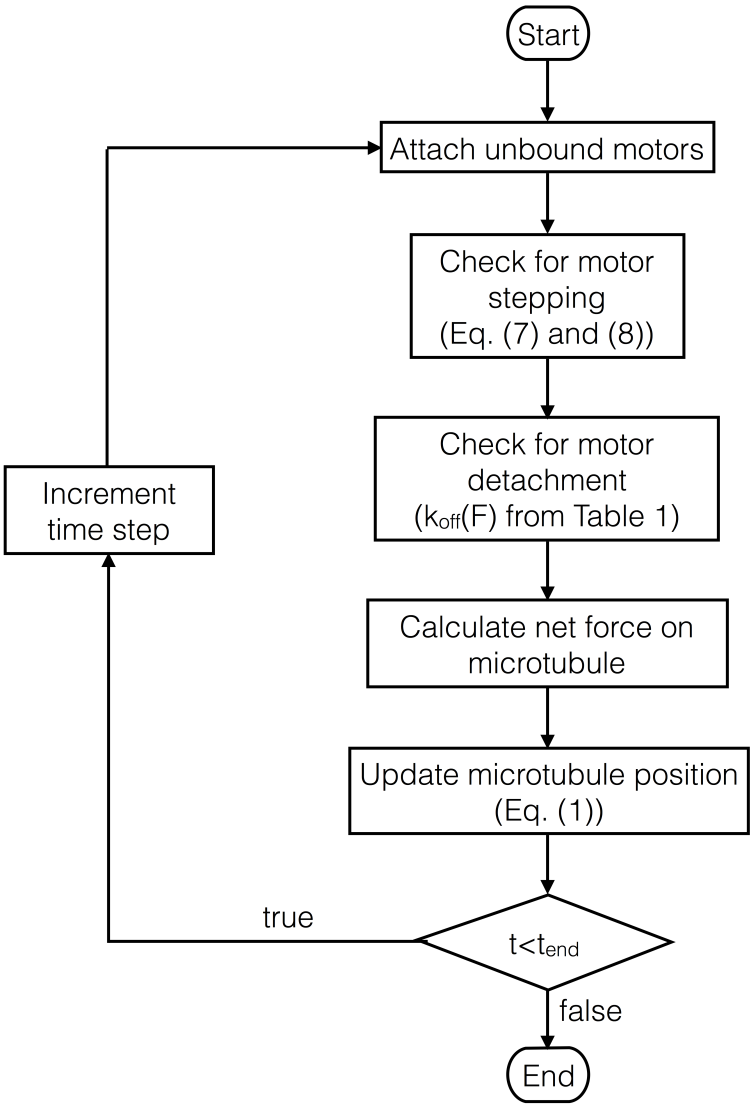

Figure S10: Flow chart describing the gliding assay simulations.

References

[1] Driver, J. W., A. R. Rogers, D. K. Jamison, R. K. Das, A. B. Kolomeisky, and M. R. Diehl, 2010. Coupling between motor proteins determines dynamic behaviors of motor protein assemblies. Phys Chem Chem Phys 12:10398–10405.

[2] Driver, J. W., D. K. Jamison, K. Uppulury, A. R. Rogers, A. B. Kolomeisky, and M. R. Diehl, 2011. Productive cooperation among processive motors depends inversely on their mechanochemical efficiency. Biophys J 101:386–395.

[3] Myers, K. A., and P. W. Baas, 2007. Kinesin-5 regulates the growth of the axon by acting as a brake on its microtubule array. J Cell Biol 178:1081–1091.

[4] Ferenz, N. P., A. Gable, and P. Wadsworth, 2010. Mitotic functions of kinesin-5. Semin Cell Dev Biol 21:255–259.

[5] Coy, D. L., W. O. Hancock, M. Wagenbach, and J. Howard, 1999. Kinesin's tail domain is an inhibitory regulator of the motor domain. Nature Cell Biology 1:288–292.

[6] Kerssemakers, J., J. Howard, H. Hess, and S. Diez, 2006. The distance that kinesin-1 holds its cargo from the microtubule surface measured by fluorescence interference contrast microscopy. Proc Natl Acad Sci U S A 103:15812–15817.

[7] Shastry, S., and W. O. Hancock, 2011. Interhead tension determines processivity across diverse N-terminal kinesins. Proc Natl Acad Sci U S A 108:16253–16258.

[8] Yardimci, H., M. van Duffelen, Y. Mao, S. S. Rosenfeld, and P. R. Selvin, 2008. The mitotic kinesin CENP-E is a processive transport motor. Proc Natl Acad Sci U S A 105:6016–6021.

[9] Valentine, M. T., P. M. Fordyce, T. C. Krzysiak, S. P. Gilbert, and S. M. Block, 2006. Individual dimers of the mitotic kinesin motor Eg5 step processively and support substantial loads in vitro. Nat Cell Biol 8:470–476.

[10] Andreasson, J. O. L., 2013. Single-molecule biophysics of kinesin family motor proteins. Phd thesis, Stanford University, California.

[11] Svoboda, K., P. Mitra, S. M. Block, 1994. Fluctuation analysis of motor protein movement and single enzyme kinetics. Proc Natl Acad Sci U S A 91:11782–11786.

Supplemental Movie Legends

Movie S1. Movie from a uniform kinesin-1 simulation. Motor tethers are shown as red springs that are partially transparent until stretched beyond their 40 nm rest length. A portion of the microtubule (green) is shown, plus-end is at left. Motor density is artificially chosen to be high ($\rho = 40\ \mu m^{-1}$) for better visualization. Microtubule diameter and height, and kinesin tether are to scale, but motor heads and tail (yellow) are not. Frame rate is 20 fps.

Movie S2. Movie from a uniform kinesin-2 simulation. Motor tethers are shown as red springs that are partially transparent until stretched beyond their 40 nm rest length. A portion of the microtubule (green) is shown, plus-end is at left. Motor density is artificially chosen to be high ($\rho = 40\ \mu m^{-1}$) for better visualization. Microtubule diameter and height, and kinesin tether are to scale, but motor heads and tail (yellow) are not. Frame rate is 20 fps.

Movie S3. Movie from a uniform kinesin-3 simulation. Motor tethers are shown as red springs that are partially transparent until stretched beyond their 40 nm rest length. A portion of the microtubule (green) is shown, plus-end is at left. Motor density is artificially chosen to be high ($\rho = 40\ \mu m^{-1}$) for better visualization. Microtubule diameter and height, and kinesin tether are to scale, but motor heads and tail (yellow) are not. Frame rate is 20 fps.

Movie S4. Movie from a uniform kinesin-5 simulation. Motor tethers are shown as red springs that are partially transparent until stretched beyond their 40 nm rest length. A portion of the microtubule (green) is shown, plus-end is at left. Motor density is artificially chosen to be high ($\rho = 40\ \mu m^{-1}$) for better visualization. Microtubule diameter and height, and kinesin tether are to scale, but motor heads and tail (yellow) are not. Frame rate is 20 fps.

Movie S5. Movie from a uniform kinesin-7 simulation. Motor tethers are shown as red springs that are partially transparent until stretched beyond their 40 nm rest length. A portion of the microtubule (green) is shown, plus-end is at left. Motor density is artificially chosen to be high ($\rho = 40\ \mu m^{-1}$) for better visualization. Microtubule diameter and height, and kinesin tether are to scale, but motor heads and tail (yellow) are not. Frame rate is 20 fps.

Movie S6. Movie from a 50/50 kinesin-1/kinesin-2 simulation. Kinesin-1 and kinesin-2 are shown in red and blue, respectively. Motor tethers are partially transparent until stretched beyond their 40 nm rest length. A portion of the microtubule (green) is shown, plus-end is at left. Motor density is artificially chosen to be high ($\rho = 40\ \mu m^{-1}$) for better visualization. Microtubule diameter and height, and kinesin tether are to scale, but motor heads and tail (yellow) are not. Frame rate is 20 fps.

Movie S7. Movie from a 50/50 kinesin-1/kinesin-3 simulation. Kinesin-1 and kinesin-3 are shown in red and blue, respectively. Motor tethers are partially transparent until stretched beyond their 40 nm rest length. A portion of the microtubule (green) is shown, plus-end is at left. Motor density is artificially chosen to be high ($\rho = 40\ \mu m^{-1}$) for better visualization. Microtubule diameter and height, and kinesin tether are to scale, but motor heads and tail (yellow) are not. Frame rate is 20 fps.

Movie S8. Movie from a 50/50 kinesin-1/kinesin-5 simulation. Kinesin-1 and kinesin-5 are shown in red and blue, respectively. Motor tethers are partially transparent until stretched beyond their 40 nm rest length. A portion of the microtubule (green) is shown, plus-end is at left. Motor density is artificially chosen to be high ($\rho = 40\ \mu m^{-1}$) for better visualization. Microtubule diameter and height, and kinesin tether are to scale, but motor heads and tail (yellow) are not. Frame rate is 20 fps.

Movie S9. Movie from a 50/50 kinesin-1/kinesin-7 simulation. Kinesin-1 and kinesin-7 are shown in red and blue, respectively. Motor tethers are partially transparent until stretched beyond their 40 nm rest length. A portion of the microtubule (green) is shown, plus-end is at left. Motor density is artificially chosen to be high ($\rho = 40\ \mu m^{-1}$) for better visualization. Microtubule diameter and height, and kinesin tether are to scale, but motor heads and tail (yellow) are not. Frame rate is 20 fps.

Movie S10. Movie from a 50/50 kinesin-2/kinesin-3 simulation. Kinesin-2 and kinesin-3 are shown in red and blue, respectively. Motor tethers are partially transparent until stretched beyond their 40 nm rest length. A portion of the microtubule (green) is shown, plus-end is at left. Motor density is artificially chosen to be high ($\rho = 40\ \mu m^{-1}$) for better visualization. Microtubule diameter and height, and kinesin tether are to scale, but motor heads and tail (yellow) are not. Frame rate is 20 fps.

Movie S11. Movie from a 50/50 kinesin-2/kinesin-5 simulation. Kinesin-2 and kinesin-5 are shown in red and blue, respectively. Motor tethers are partially transparent until stretched beyond their 40 nm rest length. A portion of the microtubule (green) is shown, plus-end is at left. Motor density is artificially chosen to be high ($\rho = 40\ \mu m^{-1}$) for better visualization. Microtubule diameter and height, and kinesin tether are to scale, but motor heads and tail (yellow) are not. Frame rate is 20 fps.

Movie S12. Movie from a 50/50 kinesin-3/kinesin-5 simulation. Kinesin-3 and kinesin-5 are shown in red and blue, respectively. Motor tethers are partially transparent until stretched beyond their 40 nm rest length. A portion of the microtubule (green) is shown, plus-end is at left. Motor density is artificially chosen to be high ($\rho = 40\ \mu m^{-1}$) for better visualization. Microtubule diameter and height, and kinesin tether are to scale, but motor heads and tail (yellow) are not. Frame rate is 20 fps.

Movie S13. Movie from a 50/50 kinesin-3/kinesin-7 simulation. Kinesin-3 and kinesin-7 are shown in red and blue, respectively. Motor tethers are partially transparent until stretched beyond their 40 nm rest length. A portion of the microtubule (green) is shown, plus-end is at left. Motor density is artificially chosen to be high ($\rho = 40\ \mu m^{-1}$) for better visualization. Microtubule diameter and height, and kinesin tether are to scale, but motor heads and tail (yellow) are not. Frame rate is 20 fps.

Movie S14. Movie from a 50/50 kinesin-5/kinesin-7 simulation. Kinesin-5 and kinesin-7 are shown in red and blue, respectively. Motor tethers are partially transparent until stretched beyond their 40 nm rest length. A portion of the microtubule (green) is shown, plus-end is at left. Motor density is artificially chosen to be high ($\rho = 40\ \mu m^{-1}$) for better visualization. Microtubule diameter and height, and kinesin tether are to scale, but motor heads and tail (yellow) are not. Frame rate is 20 fps.